GAP CLEARING KICKER MAGNET FOR MAIN INJECTOR

C. C. Jensen, R. Reilly, I. Terechkine, Fermilab*, Batavia IL USA 60510

Abstract

A new fast extraction kicker magnet is required to clear the injection gap in the Main Injector at FNAL. An overview of the design choices is presented and the results of testing of the first prototype are discussed.

1 INTRODUCTION

These kicker system requirements were originally conceived for the NOvA project, a neutrino experiment located in Minnesota. To achieve the desired neutrino flux, several upgrades are required to the Main Injector (MI) accelerator and Recycler storage ring (RR) at Fermilab. One of these changes is a new gap clearing kicker in RR to reduce activation from beam loss. This new kicker will be used to extract uncaptured beam, created during the slip stack injection process [1], down the existing abort line. The MI would benefit from this gap clearing system immediately. A decision was made that early installation would be done in MI before moving the system to RR during NOvA. An identical system will be built for injection into the RR. Table 1 summarizes requirements for the kickers.

Table 1. Kicker System Requirements

	MI Gap Clearing	RR Gap Clearing	RR Injection
Angle	1.70 mrad	1.18 mrad	1.21 mrad
Field Rise	57 ns	57 ns	57 ns
Field Fall	400 ns	57 ns	57 ns
Pulse Width Duty Factor	1534 ns at 15 Hz burst rate 12 pulses per 1.33 seconds		
Stability	±3% of Nom. Flattop plus Pulse to Pulse		
Stability	±3% of Nom. Max. to Circulating Beam		
Beam Aperture	33 mm (perpendicular to kick) x 81 mm (parallel to kick)		

2 SYSTEM DESIGN

The MI gap clearing kicker system inherits features of previous fast kicker magnets [2, 3]. A thyratron switch will be used with coaxial cable pulse forming line (PFL). The cable will be pulse charged so that the thyratron can be run at high reservoir, and therefore high speed. The magnet will have a ceramic chamber with the required beam aperture. To fit the vacuum chamber, the magnetic aperture must be 53 mm x 110 mm. It will be a travelling wave magnet. The load, matched to the cable impedance, will be mounted to the end of the magnet. Because a variety of repetition rates are expected, the effect of average power on the magnet termination resistance has to be limited to ~1%. This has been done successfully on previous systems [4]. We will use the same magnet to meet the requirements for the three systems in Table I.

* Fermilab is operated by Fermi Research Alliance, LLC. under Contract No. DE-AC02-07CH11359 with the US Department of Energy

Given a previously demonstrated pulser voltage rise time (3% to 97%) of ~25 ns, the magnet fill time must be less than 32 ns to meet the field rise time requirement. As we rely on 50 Ω cable, the choices for the kicker impedance Z0 are 50 Ω, 50/2 Ω, 50/3 Ω, etc. Vacuum and HV connections add ~0.5 m to the magnet length. Using 25 Ω or lower impedance would result in a lower ratio of the kicker magnetic length to its physical length. With the required aperture, rise time and 50 Ω impedance, the magnetic length is ~0.7 m. A maximum operating voltage of 55 kV on the thyratron then determines the maximum kick of 275 μrad per magnet.

While the rise and fall time for MI use are comparable to a previous kicker [2], meeting the fall time will be a new issue for the RR kickers. These kickers need a "bumper" system to cancel the tail and allow the system to meet the fall time requirement to the 3% level. The kicker system will consist of a pulsed power supply driving an additional kicker magnet mounted upside down and backwards in the tunnel. This requires complete mechanical symmetry in the magnet and is the final constraint on the magnet design.

3 MAGNET SIMULATION

3.1 Circuit Simulation

The first step in detailed design is a circuit simulation of the proposed magnet. It is known that parasitic elements in the magnet unit cell limit the bandwidth [5]. SPICE version 3F5 was used to simulate the magnet, including parasitic elements, mainly capacitor inductance and cell-to-cell coupling, from previous similar designs. The cell length is a series of tradeoffs between high voltage hold off of the capacitor bus, field uniformity, required capacitance and manufacturing capability. This simulation showed that the rise time could be achieved with less than 30 cells of 2.3 cm long. The final design has 27 ferrites and a stacking factor of 72%, which does not change the integrated field substantially and maintains adequate high voltage clearance for the capacitor bus (see Fig. 3).

The kicker design has to ensure a special value of the end capacitance. SPICE simulations of the magnet clearly showed a decrease in the field rise time when the end capacitance was between 50 and 60 pF. This value depends on input and output inductance and impedance match, but much larger or smaller capacitance values increase 3%–97% field rise time.

3.2 Field Simulation

Capacitor design was the most technically challenging part of the magnet. The capacitor had to have a tight tolerance on value, a long life and a low series

inductance. The tight tolerance on the capacitance value required more than tight mechanical tolerances (+/- 80 μm). A 3D simulation of a cell of the magnet was ultimately done using COMSOL [6]. Approximately 15% of the capacitance is not from the HV capacitor electrode. Confidence in the modelling results was obtained by comparing the model with measurements on the prototype. The electrode design was for a peak electric field of not more than 9 kV/mm at a nominal voltage of 26 kV. A previous magnet [2] was designed, 2D, for a peak field of 8 kV/mm at 25 kV, and there have been no failures in $7{\cdot}10^8$ pulses at that voltage. The new limit is about 30% of the material breakdown, which under ASTM test method D149 is ~21 kV_{rms}/mm. An operating level of 30% to 50% of breakdown is preferred to allow for surface imperfections. The capacitor inductance was kept low by making the conductor wide enough between the ferrites so it extended past the edge of the flux return.

The ferrite cell was also simulated using COMSOL. One concern was high frequency dimensional resonance inside the ferrite itself. This resonance can appear in high permeability material with large sections. A study showed that with μ of 1500 and ε of 15, resonances can occur in the 40-50 MHz range. While permeability falls at these frequencies, a lower permeability material (μ = 400) was chosen to lessen this effect. The smallest ferrite cross-section without significant saturation was also chosen.

One must also be able to adjust the average impedance of the magnet due to normal variations in capacitance and inductance. This adjustment is accomplished by trimming the low voltage bus, Fig. 3, which changes the inductance. This trimming is limited to about ±5% in inductance so it is also important to get the capacitance and inductance as close as possible to nominal values.

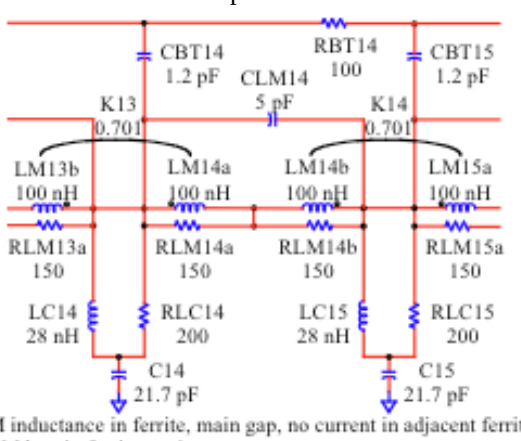

LM inductance in ferrite, main gap, no current in adjacent ferrite
RLM loss in ferrite, main gap
LC inductance in capacitor bus, between ferrites
RLC loss in ferrite, capacitor bus
K coupling between adjacent ferrites, SPICE definition
C main capacitor
CBT capacitance from HV bus to coating inside vacuum chamber
RBT resistance of coating inside vacuum chamber
CLM capacitance between adjacent capacitor buses

Fig. 2, Equivalent Circuit; Two Mid-Magnet Cells

4 PROTOTYPING

The prototype magnet was built for several purposes: to determine the best ferrite material, to validate the field modelling, to validate the circuit modelling and to perform high voltage life testing. The ferrite material chosen was based on performance in the prototype magnet. Testing of three materials, with μ of 300, 400 and 550, showed that magnet cells made with μ of 400 had the lowest overshoot at the output. We believe this is mainly due to higher ferrite losses.

The circuit model shown in Fig. 2 was based on measurements from the prototype magnet. This model is significantly different from the original design model in that the stray inductance (LC) is much less, the coupling (K) between cells is higher and of the opposite polarity**,** and the equivalent ferrite loss (RLM) is much higher. While the values of LC, LM, K, C, CBT and RBT in Fig. 2 are based on measurements, RLM and RLC are chosen for a best fit of simulation to the measurements. These parameters are frequency dependant, but this feature was not included in the model. Since lossy dispersion was not done correctly, there is a poor match of the output voltage rise time between modelled (29 ns) and measured (37 ns).

Validation of the electric field simulations of the cell capacitance was most critical. A model of a bare HV bus cell was compared to measurements of the bare HV bus with ends. Careful measurements of the capacitance at the ends of the magnet were also made. The total measured capacitance was 6 pF larger than the total of prediction from model plus end measurements. This difference was attributed to the end but was not verified by modelling to find a source of the discrepancy. The model prediction for the prototype configuration was 21.5 pF per cell with potting ε of 2.74 and ferrite ε of 14. The measurement gave a value of 21.9 pF, including the end correction above, with estimated potting ε of 2.74. One possible source for this difference is the procedure to extract the cell capacitance from the measured total magnet capacitance. Another source can be the dielectric properties of the ferrite material, which contribute about 9% to the total cell capacitance, but are not well controlled.

The dielectric constant for the potting material, Sylgard 184, was also determined from measured capacitance before and after potting. The data sheet ε is 2.75 when cured at 65 C for 4 hours. Initially, ε was 2.79 and came down to 2.73 after 4 months, but it was cured at room temperature. This is done to prevent the potting from pulling away from the materials with different expansion coefficients as the magnet cools. This separation could cause air gaps to form and compromise the insulation.

High voltage testing of the prototype was done for about 4 months at the nominal repetition rate. The magnet was driven at 26 kV for $2{\cdot}10^7$ pulses and at 30 kV for 10^7 pulses without any failures. Because this is only 1% of

the desired lifetime, 60 Hz corona testing of the prototype and first production magnet are to take place shortly.

Following the high voltage pulse testing of the magnet, final changes were made to the drawings and almost all parts for the eight production magnets were ordered. The final magnet cross sections are shown in Fig 3.

While measurements showed fairly good agreement with the model, it is still possible to get outside the desired capacitance range; therefore capacitors for only the first three magnets were ordered so that production could start.

Pulse testing of the first production magnet has just recently begun. The inductance, capacitance and complex impedance were measured with an AC impedance bridge. A procedure for adjusting the magnet impedance by trimming the low voltage bus was carried out which achieved 50 Ω at 1 V_{rms}. The magnet was then moved to a high voltage testing area with an existing pulser. Measuring the reflection from the high power load at 6 kV, the impedance is about 52 Ω and at 24 kV, the impedance is about 53 Ω. The impedance match should be closer, but the capacitance between HV bus and beam tube was much lower than in the prototype. A slight mismatch between load and magnet (with the load being 2% smaller) reduces the field rise time. However, there was a substantial undershoot (~10%) on magnet input voltage due to excessive capacitance at the load. The capacitance of the load was much larger than estimated. The SPICE model was then modified to match the measurement and the effective capacitance of the load was determined. The input (and output) capacitance will now be changed for the remaining magnets to produce the desired response, shown in Fig. 4. Further details on simulations and measurements are included in the design report [7].

5 CONCLUSIONS

The magnet parameters and performance of the system has been compared to the models. We expect that the performance specifications will be met with the slight end modification and production will continue. Seven magnets are scheduled to be installed summer of 2009 in MI and six more magnets, including the bumper, are scheduled for installation in the RR in early 2012.

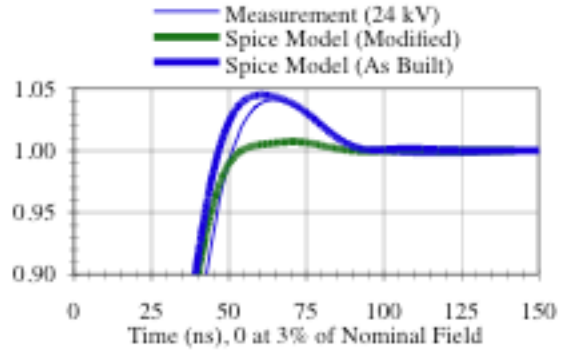

Fig. 4. Comparison of Integrated Magnetic Field Measurement and Model; Model w/ Reduced Capacitance

This magnet collaboration was across two divisions and four groups at Fermilab. Thanks to all who contributed thoughts and effort.

6 REFERENCES

[1] K. Seiya, “Progress in Multi-Batch Slip Stacking in the Fermilab Main Injector and Future Plans”, PAC2009

[2] D. Qunell, C. Jensen, D. Tinsley, “Kicker System for 8 GeV Proton Injection”, PAC1997, pp1287-1289

[3] C. Jensen, B. Hannah, R. Reilly, “A Fast Injection Kicker for the Tevatron”, PAC2001, pp3720-3723

[4] S. Reeves, C. Jensen, “Numi Proton Kicker Extraction Magnet Termination Resistor System”, PAC2005, pp2224-2226

[5] G. Nassibian, “Traveling Wave Kicker Magnets with Sharp Rise and Less Overshoot”, IEEE Trans. Nucl. Sci., Vol 26,pp.4018-4020,1979

[6] COMSOL, Vers. 3.4, Multiphysics with AC/DC Module, COMSOL Inc, Burlington MA 01803

[7] C. Jensen, MI Gap Clearing Kicker Magnet Design Review, Fermilab TM-2429-AD

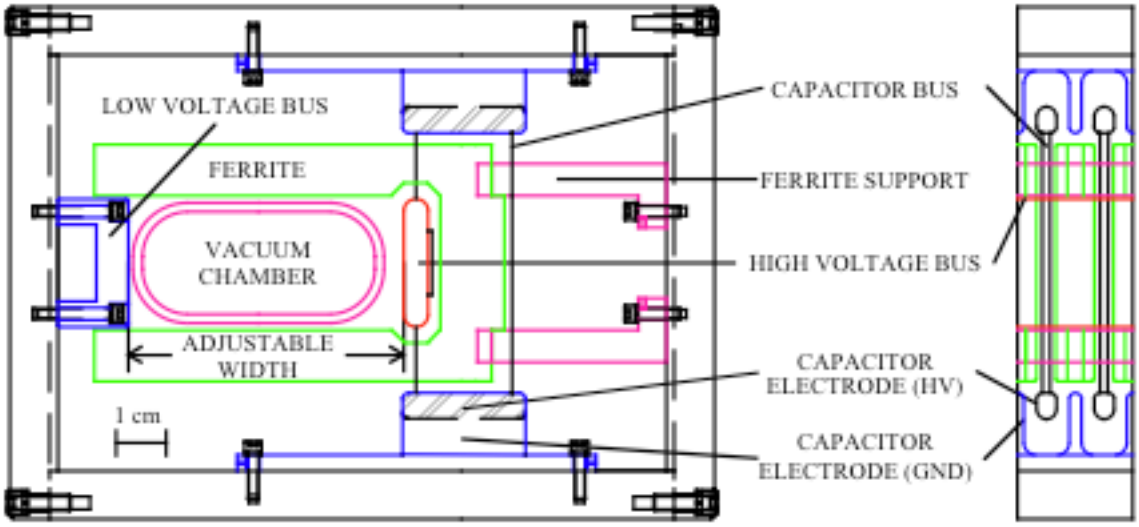

Fig. 3, Cross Section of the Kicker Magnet